

Original paper

Dose uncertainty due to energy dependence in dual-energy computed tomography

Daisuke Kawahara^{1*,A,B,C,D,E,F}, Takatoshi Toyoda^{2*,A,B,C,E}, Kazushi Yokomachi^{2,A}, Chikako Fujioka^{2,A}, Yasushi Nagata^{1,3,A}

¹Department of Radiation Oncology, Institute of Biomedical & Health Sciences, Hiroshima University, Hiroshima City, Japan

²Radiation Therapy Section, Division of Clinical Support, Hiroshima University Hospital, Hiroshima City, Japan

³Hiroshima High-Precision Radiotherapy Cancer Centre, Hiroshima City, Japan

*Both authors contributed equally to this manuscript.

Abstract

Purpose: To evaluate the absolute dose uncertainty at 2 different energies and for the large and small bowtie filters in dual-energy computed tomography (DECT).

Material and methods: Measurements were performed using DECT at 80 kV and 140 kilovoltage peak (kVp), and single-energy computed tomography (CT) at 120 kV. The absolute dose was calculated from the mass-energy absorption obtained from the half-value layer (HVL) of aluminium.

Results: The difference in the water-to-air ratio of the mean mass energy-absorption coefficients at 80 kV and 140 kV was 2.0% for the small bow-tie filter and 3.0% for the large bow-tie filter. At lower tube voltages, the difference in the absorbed dose with the large and small bow-tie filters was larger.

Conclusions: The absolute dose uncertainty due to energy dependence was 3.0%, which could be reduced with single-energy beams at 120 kV or by using the average effective energy measurement with dual-energy beams.

Key words: dual-energy CT, energy absorption coefficient.

Introduction

Dual-energy computed tomography (DECT) can be used to discriminate tissues and characterize tissue composition based on the principle that materials have different attenuations at different energies. Clinically, it is applied for the automatic characterization of kidney stones, visualization of lung perfused blood volume and ventilation, and automatic removal of bone [1-5]. DECT can be used to obtain the electron density, effective atomic number, and monochromatic computed tomography (CT) number by exploiting the attenuation differences in tissues to improve material decomposition [6,7]. In our previous study, we developed a material decomposition system for

contrast agents using DECT [8,9]. Thus, DECT has been increasingly used in the clinical setting to improve the accuracy of lesion detection.

Prior studies have evaluated the image quality of DECT using phantom scans, simulations, and patients [10-15]. However, radiation dose in DECT is a problem because DECT uses two X-ray tubes with different tube voltages. Some groups have compared the radiation dose of DECT and conventional single-energy CT (SECT) [16,17]. Reportedly, the dose in DECT was nearly 2 times higher than that in SECT. In DECT, the tube currents of both the tubes are adapted to achieve comparable noise levels. Moreover, bow-tie filters shape the photon beam and reduce beam hardening and the radiation dose [18].

Correspondence address:

Daisuke Kawahara, PhD, Radiation Therapy Section, Department of Clinical Support, Hiroshima University Hospital, 1-2-3 Kasumi, Minami-ku, Hiroshima City 734-8551, Japan, e-mail: daika99@hiroshima-u.ac.jp

Authors' contribution:

A Study design · B Data collection · C Statistical analysis · D Data interpretation · E Manuscript preparation · F Literature search · G Funds collection

The energy mass absorption coefficient and the ratio of the beam pulse for each energy level used in DECT are required to derive the radiation dose. The difference in the energy mass absorption coefficient owing to the tube voltages and the type of bow-tie filters affect the uncertainty of the dose measurement in DECT. The energy absorption coefficient and electric current or charge must be measured to calculate the imaging dose.

The objectives of the current study were to evaluate the difference in the energy mass absorption and absolute dose due to the tube voltages and bow-tie filters in DECT.

Material and methods

DECT scans were performed with a Revolution CT scanner (GE Healthcare, Princeton, NJ, USA), which is a single-source scanner with kV switching. The tube voltages were set to 80 kV, 120 kV, and 140 kV and exposure to 150 mA using the sequential scan mode.

Effective energy

The effective energy was obtained from the half-value layer (HVL) of aluminium (Al). The experimental setup for this measurement is shown in Figure 1. The beam collimation was set to 8×0.625 mm. The chamber, which is a 0.6 cc farmer-type air ionization chamber (PTW 30013), is located at the isocentre. The amount of charge was measured by varying the thickness of the aluminium plate where the tube was stationary. The HVL was measured for the tube voltages in DECT, which were 80 kV and 140 kV, and in conventional SECT, which was 120 kV. DECT can be used to select small and large bow-tie filters. The dif-

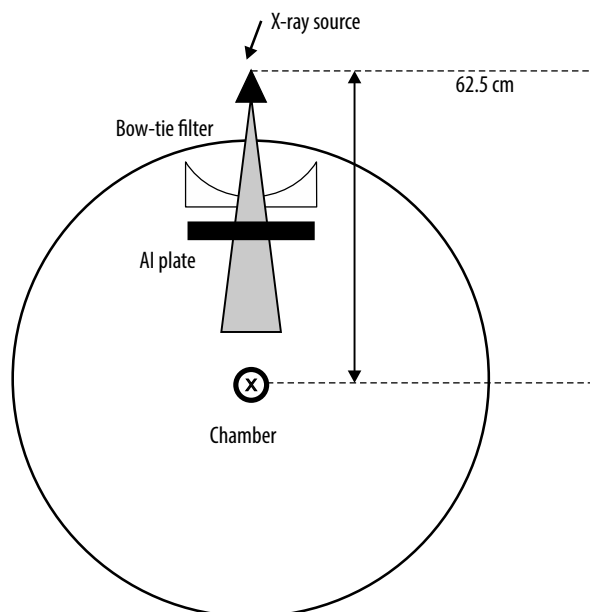


Figure 1. Experimental setup of the half-value layer (HVL) measurement. The chamber is located at the isocentre, and the amount of charge is measured by varying the aluminium plate thickness

ference in the HVL between the small and large bow-tie filters was also evaluated. The effective energies were calculated using the basic data from Selzer and Hubbell [19].

Chamber correction factor and absolute dose measurement

A schematic diagram of the measurement setup is shown in Figure 2. The chamber is located at the isocentre. The small and large bow-tie filters were used, and the beam collimation was set to 256×0.625 mm. The effective energy was obtained from the HVL. The absorbed dose to water (D_w) was derived as follows:

$$D_w = M \times N_k \times k_{TP} \times B \times [(\mu_{en}/\rho)_{w,air}], \quad (1)$$

where N_k is the air-kerma calibration factor for a given beam quality; M , the chamber reading measured in the farmer chamber with the build-up cap at the isocentre; B , the water-to-air ratio of the mean mass energy-absorption coefficients averaged over the incident X-ray spectrum; and k_{TP} , the backscattering factor, which was defined in a previous study [20]. The absorbed dose was calculated for the tube voltages in DECT, which were 80 kV and 140 kV, and in conventional SECT, which was 120 kV, with the large and small bow-tie filters, using equation (1).

Dose profile with the bow-tie filters

The off-centre ratio (OCR) in the air was measured, as shown in Figure 3. The small and large bow-tie filters were used, and the beam collimation was set to 256×0.625 mm. The OCR profile covered by the half-fan beam was measured up to a distance of 25.0 cm from the isocentre in 5-10-mm intervals along the vertical axis across the fan beam at 120 kV. OCRs were compared between the large and small bow-tie filters.

Results

HVL, effective energy, and water-to-air ratio of the mean mass energy-absorption coefficients

Figure 4 shows the correlation between the relative dose and the thickness of the aluminium plate at 80 kV, 120 kV, and 140 kV. The HVL, effective energy, and water-to-air ratio of the mean mass energy-absorption coefficients are listed in Table 1. The HVL and effective energy were higher at higher tube voltages. The difference in the water-to-air ratio of the mean mass energy-absorption coefficients at 80 kV and 140 kV was 2.0% for the small bow-tie filter and 3.0% for the large bow-tie filter. The difference in the water-to-air ratio of the mean mass energy-absorption coefficients at 80 kV and 120 kV was 0.6% for the small bow-tie filter and 0.6% for the large bow-tie filter. The difference in the water-to-air ratio of the mean mass energy-

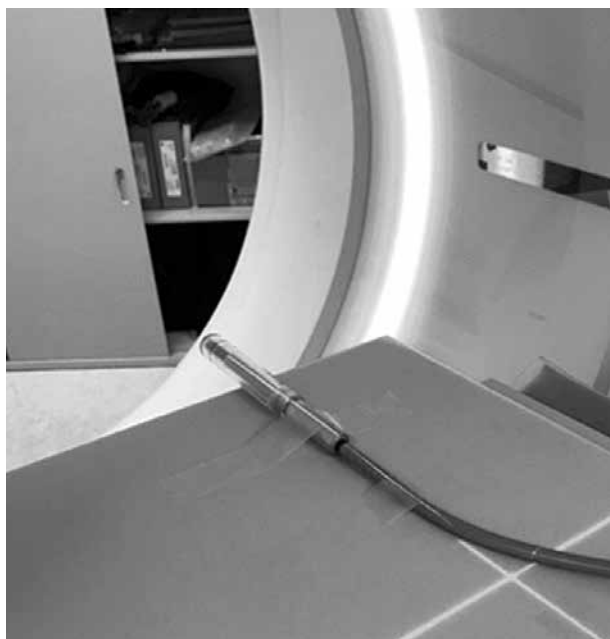


Figure 2. Experimental setup of the absolute dose measurement. The chamber with the build-up cap is located at the isocentre, and the amount of charge is measured

absorption coefficients at 120 kV and 140 kV was 1.4% for the small bow-tie filter and 2.1% for the large bow-tie filter. The HVL and effective energy with the large bow-tie filter were higher than those with the small bow-tie filter for all the tube voltages. The difference in the water-to-air ratio of the mean mass energy-absorption coefficients with the large and small bow-tie filters was within 1.0% for all the tube voltages.

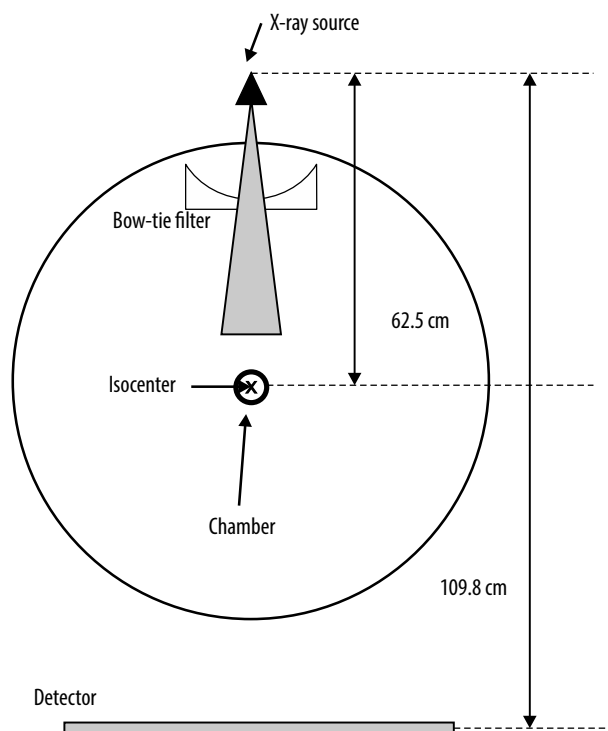
Absolute dose difference due to bow-tie filters

Figure 5 shows the comparison of OCR profiles between the large and small bow-tie filters in the air. The centre dose was higher with the small bow-tie filter than with the large bow-tie filter. However, the penumbra was larger with the large bow-tie filter than with the small bow-tie filter. Table 2 shows the absorbed dose with the large and small bow-tie filters at 80 kV, 120 kV, and 140 kV. Figure 6 shows the dose difference between the large and small bow-tie filters at the isocentre, which was larger at the lower tube voltages.

Discussion

DECT uses different tube voltages, allowing material characterization based on differences in the material and tissue attenuation. The current study evaluated the difference in effective energy between low and high tube voltages in DECT.

The HVL and effective energy were significantly higher at higher tube voltages. The American Association of Physicists in Medicine Task Group 61 report showed that the uncertainty of the water-to-air ratio of the mean



mass energy-absorption coefficients was 1.5% in kV X-ray beams [21]. In the current study, the difference in the water-to-air ratio for the mean mass energy-absorption coefficients at 80 kV and 140 kV was 2.0% with the small bow-tie filter and 3.0% with the large bow-tie filter. These differences were larger than the uncertainty in the absolute dose measurement.

The ratio of the dose at 80 kV and 140 kV X-ray beams cannot be measured separately in clinical DECT measurements. The uncertainty of the absorbed dose

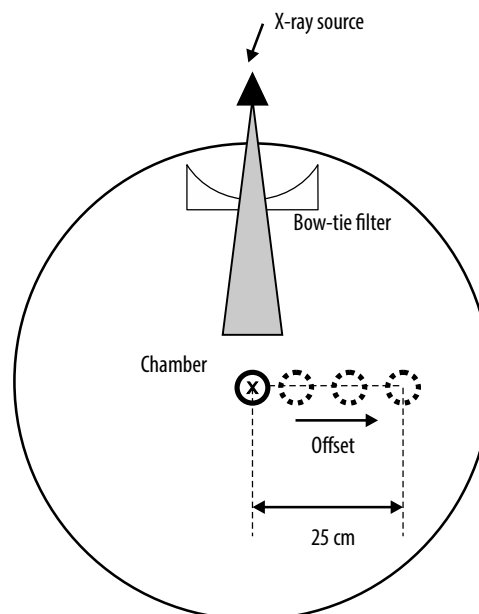


Figure 3. Experimental setup of the off-centre ratio (OCR) measurement. The chamber is offset from the isocentre along the vertical axis across the fan beam at 120 kV

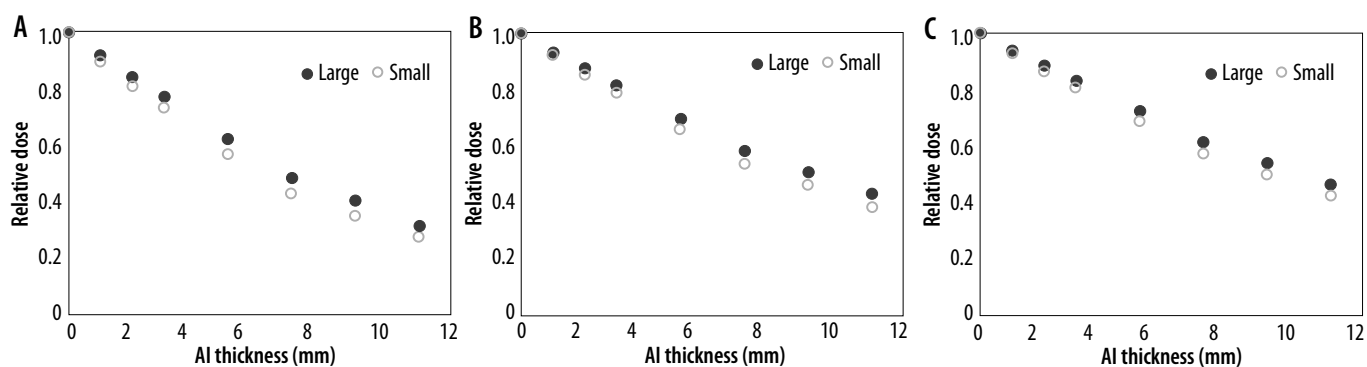


Figure 4. Correlation of the relative dose and the thickness of the aluminium plate at (A) 80 kV, (B) 120 kV, and (C) 140 kV

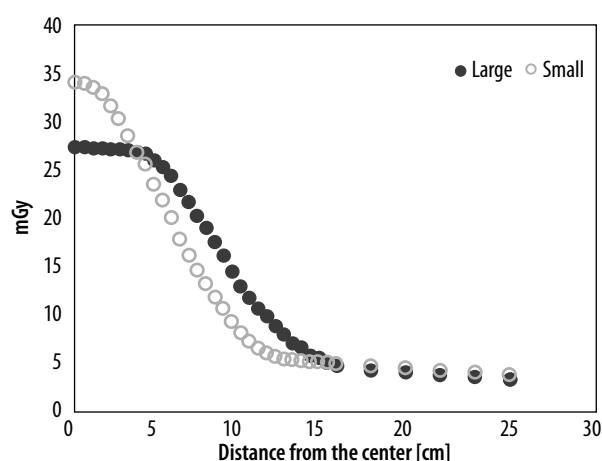


Figure 5. Comparison of the off-centre ratio (OCR) profiles with the large and small bow-tie filters

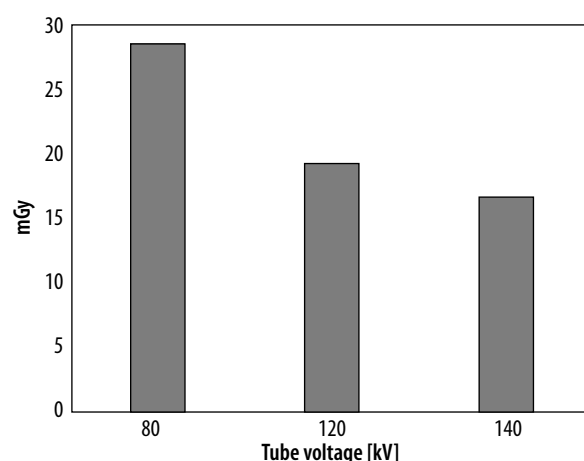


Figure 6. Absolute dose difference between the large and small bow-tie filters at 80-140 kV

Table 1. Half-value layer (HVL), effective energy, and the water-to-air ratio of the mean mass energy-absorption coefficients

Parameter	80 kV		120 kV		140 kV	
	Large	Small	Large	Small	Large	Small
Bowtie filter	Large	Small	Large	Small	Large	Small
Al HVL [mm]	7.08	6.09	9.20	8.13	10.0	8.96
Effective energy [keV]	48.5	46.8	56.9	52.3	59.7	55.9
$\frac{(\mu_{en}/\rho)_{water}}{(\mu_{en}/\rho)_{air}}$	1.02	1.02	1.04	1.03	1.05	1.04

Table 2. Absorbed dose with the large and small bow-tie filters at the isocentre at 80-140 kV

Dose	Large (mGy)	Small (mGy)
80 kV	14.1	19.4
120 kV	39.7	48.7
140 kV	55.7	66.2

measurement due to energy dependence can be reduced by 1.4% with the small bow-tie filter and 2.1% with the large bow-tie filter using the water-to-air ratio of the mean mass energy-absorption coefficients at 120 kV. Moreover, Raudabaugh *et al.* investigated the internal dose with a metal-oxide-semiconductor field-effect transistor (MOSFET) dosimeter in DECT [21]. They evaluated the

dose equivalence between the MOSFET and an ion chamber [22] and calculated a linear attenuation coefficient using a simple relation by directly measuring the HVL of the combined dual-energy beams. The Monte Carlo calculation is another method to reduce the energy dependence of DECT. It is a powerful tool for examining the impact of different energy beams and an individual's anatomy on patient dose [22].

The effect of differences in the bow-tie filter on the dose measurement was small for all the tube voltages. Thus, the same mass energy-absorption coefficient can be used for dose measurements for both large and small bow-tie filters. However, the dose difference at the isocentre between the large and small bowtie filters was higher at lower tube voltages. The photon energy is decreased by the bow-tie filter, which causes beam hardening.

The beam hardening is higher with lower photon energy and reduces the absorbed dose. The limitation of the current study was the relationship between image quality and the absorbed dose in DECT. Further studies must be performed to evaluate the image quality and organ dose using the dose measurement with reduced uncertainty in DECT.

Conclusion

In the current study, the difference in the mass energy absorption was small (within 1.0%). The uncertainty of

the absolute dose was increased by 3.0% using mass-energy absorption with either a low or high tube voltage in DECT. The uncertainty of mass-energy absorption due to energy dependence can be decreased by using the average effective energy with dual-energy beams.

Conflict of interest

The authors report no conflict of interest.

References

1. Kaemmerer N, Brand M, Hammon M, et al. Dual-energy computed tomography angiography of the head and neck with single-source computed tomography: a new technical (split filter) approach for bone removal. *Invest Radiol* 2016; 51: 618-623.
2. Primak AN, Fletcher JG, Vrtiska TJ, et al. Noninvasive differentiation of uric acid versus nonuric acid kidney stones using dual-energy CT. *Acad Radiol* 2007; 14: 1441-1447.
3. Michalak G, Grimes J, Fletcher J, et al. Improved CT number stability across patient size using dual-energy CT virtual monoenergetic imaging. *Med Phys* 2016; 43: 513.
4. Chae EJ, Seo JB, Goo HW, et al. Xenon ventilation CT with a dual-energy technique of dual-source CT: initial experience. *Radiology* 2008; 248: 615-624.
5. Henzler T, Meyer M, Reichert M, et al. Dual-energy CT angiography of the lungs: comparison of test bolus and bolus tracking techniques for the determination of scan delay. *Eur J Radiol* 2012; 81: 132-138.
6. Meier A, Wurnig M, Desbiolles L, et al. Advanced virtual monoenergetic images: improving the contrast of dual-energy CT pulmonary angiography. *Clin Radiol* 2015; 70: 1244-1251.
7. Kawahara D, Ozawa S, Yokomachi K. Accuracy of the raw-data-based effective atomic numbers and monochromatic CT numbers for contrast agent with a dual-energy CT technique. *Br J Radiol* 2018; 91: 20170524.
8. Kawahara D, Ozawa S, Tanaka S, et al. Automatic contrast agent extraction system using electron density data with dual-energy CT. *Br J Radiol* 2018; 91: 20180396.
9. Kawahara D, Ozawa S, Yokomachi K, et al. Improving automatic contrast agent extraction system using monochromatic CT number. *Australas Phys Eng Sci Med* 2019; 42: 819-826.
10. Tawfik AM, Kerl JM, Razek AA, et al. Image quality and radiation dose of dual-energy CT of the head and neck compared with a standard 120-kVp acquisition. *Am J Neuroradiol* 2011; 32: 1994-1999.
11. Yu LF, Christner JA, Leng S, et al. Virtual monochromatic imaging in dual-source dual-energy CT: radiation dose and image quality. *Med Phys* 2011; 38: 6371-6379.
12. Kawahara D, Ozawa S, Yokomachi K, et al. Accuracy of the raw-data-based effective atomic numbers and monochromatic CT numbers for contrast agent with a dual-energy CT technique. *Br J Radiol* 2018; 91: 20170524.
13. Kawahara D, Ozawa S, Yokomachi K, et al. Evaluation of raw-data-based and calculated electron density for contrast media with a dual-energy CT technique. *Rep Pract Oncol Radiother* 2019; 24: 499-506.
14. Kawahara D, Ozawa S, Yokomachi K, et al. Metal artifact reduction techniques for single energy CT and dual-energy CT with various metal materials. *BJR Open* 2019; 1: 20180045.
15. Kawahara D, Ozawa S, Yokomachi K, et al. Evaluation of metal artifact techniques with same contrast scale for different commercially available dual-energy computed tomography scanners. *Phys Eng Sci Med* 2020; 43: 539-546.
16. Li B, Yadava G, Hsieh J. Quantification of head and body CTDI(VOL) of dual-energy x-ray CT with fast-kVp switching. *Med Phys* 2011; 38: 2595-2601.
17. Purysko AS, Primak AN, Baker ME, et al. Comparison of radiation dose and image quality from single-energy and dual-energy CT examinations in the same patients screened for hepatocellular carcinoma. *Clin Radiol* 2014; 69: e538-e544.
18. Aichinger H, Dierker J, Joite-Barfu B, et al. *Radiation Exposure and Image Quality in X-Ray Diagnostic Radiology, Physical Principles and Clinical Applications*. 1st ed. Springer, Berlin, Heidelberg; 2004.
19. Seltzer SM, Hubbell JH. *Tables and graphs of photon mass attenuation coefficients and mass energy-absorption coefficients for photon energies 1 keV to 20 MeV for elements Z = 1 to 92 and some dosimetric materials*. National Institute of Standards and Technology; 1995.
20. Ma CM, Coffey CW, DeWerd LA, et al. AAPM protocol for 40-300 kV X-ray beam dosimetry in radiotherapy and radiobiology. *Med Phys* 2001; 28: 868-893.
21. Raudabaugh J, Nguyen G, Lowry C, et al. Effective dose estimation from organ dose measurements in fast-kv switch dual energy computed tomography. *Radiat Prot Dosimetry* 2018; 182: 352-358.
22. Salvadó M, López M, Morant JJ, et al. Monte Carlo calculation of radiation dose in CT examinations using phantom and patient tomographic models. *Radiat Prot Dosimetry* 2005; 114: 364-368.